Water-Accelerated Photo-oxidation of $CH_3NH_3PbI_3$ Perovskite: Mechanism, rate orders, and rate constants

Timothy D. Siegler,[†a] Wiley A. Dunlap-Shohl,[†a] Yuhuan Meng,[a] Wylie F. Kau,[a] Preetham P. Sunkari,[a] Chang En Tsai,[a] Zachary J. Armstrong,[a] Yu-chia Chen,[b,c] David A. C. Beck,[a,c] Marina Meila,[d,c] Hugh W. Hillhouse*[a]

[a] Department of Chemical Engineering, Clean Energy Institute, and Molecular Engineering and Science Institute, [b] Department of Electrical and Computer Engineering, [c] eScience Institute, [d] Department of Statistics

University of Washington, Seattle, WA, United States, 98195

* Corresponding author: h2@uw.edu
[†] These authors contributed equally

Abstract

Understanding the chemical reactions that hybrid organic-inorganic halide perovskite (HP) semiconductors undergo in the presence of moisture, oxygen, and light are essential to the commercial development of HP solar cells and optoelectronics. Here we use optical absorbance to study the kinetics of methylammonium lead iodide ($MAPbI_3$) degradation in response to combinations of moisture, oxygen, and illumination over a range of temperatures. We identify two primary reaction pathways that dominate $MAPbI_3$ material degradation in these mixed environmental conditions: (1) dry photooxidation (DPO) due to the combined role of oxygen and photoexcited electrons (with a rate of 9×10^{-9} mol/m^{2}s in dry air at 25 ^{o}C and an activation energy of 0.47 eV),** and (2) a water-accelerated photooxidation (WPO) process due to the combined role of water, oxygen, and photoexcited electrons (with a rate of 1×10^{-7} mol/m^{2}s in 50% RH air at 25 ^{o}C and E_A=0.08 eV). Commonly reported humidity-only, blue light, and thermal degradation pathways are demonstrated to have rates that are respectively 100, 1000, and >1000 times slower than predominant photooxidation processes. Extracting kinetic rate constants from the dynamics of the initial degradation, we calculate that in dry air, photooxidation of $MAPbI_3$ proceeds with 1st order kinetics with respect to concentration of excess conduction band electrons and 0th order kinetics with respect to oxygen. In humid air, photooxidation of $MAPbI_3$ exhibits first order kinetics with respect to the partial pressure of water in the vapor phase (P_{H2O}). However, with respect to oxygen in the vapor phase (P_{O2}) and excess concentration of photoexcited electrons (n), kinetics follow a $kx/(1+kx)^2$ relationship with respect to rate. We then identify a plausible reaction mechanism for degradation of $MAPbI_3$ material that is consistent with these rate orders. The rate determining step for DPO is proton abstraction from methylammonium while for WPO it is proton abstraction from water, which occurs at a faster rate and results in water acting as an accelerant for photooxidation of $MAPbI_3$. Rate laws derived from this mechanism were fit to the entire dataset to extract rate constants for DPO and WPO processes. Combining the rate equations with mass transport modeling may yield mechanistic predictive models of PV device service lifetime for different encapsulation schemes. There is disagreement in the literature as to whether water is a product of DPO. If water is a product, then encapsulation regimes must be developed to rigorously block oxygen, or else, over longer time periods, water will accumulate inside the packaging and kick-off a much faster WPO process.

**** Important note related to this version of the pre-print:** We have measured ***high sensitivity to low levels of moisture*** in the degradations since the WPO is faster and lower activation energy.

For degradation runs where extra measures are taken to eliminate trace levels of moisture, the rate of reaction in "dry" air drops and the activation energy increases. When we anneal films in flowing dry N_2 to remove residual water (possibly from synthesis reagents) and then conduct the photooxidation in a mixture of ultra-dry nitrogen and ultra-dry oxygen (79% N_2, 21% O_2), the rate drops to about 3 x 10^{-9} mol/m^2s at 25 °C and the activation energy increases to 0.62 eV. The standard deviation of the rate estimates also decrease (smaller error bars in Fig 2b and 2e). The r^2 of the final parity plot is also increased. However, so that the data are self-consistent, this version of the pre-print includes results from experiments that may have had varying trace levels (~1-100 ppm) of water, and the analysis below is all from that data set. Data from more rigorous drying procedures will appear in the final version.

Introduction

Halide perovskite (HP) photovoltaics (PVs) are the first printable photovoltaic technology to achieve >25% power conversion efficiency (PCE),[1] which may allow for low-cost high-efficiency flexible PV devices fabricated by roll-to-roll printing technology.[2,3] Given the low cost of the starting materials, rigid devices such as perovskite-silicon tandems[4,5] or devices formed by vapor deposition could also lead to significant decreases in the cost of solar power if the solar cells have sufficiently long service lifetime. While a large number of studies have identified HP PV devices with >1,000 hr operational lifetimes,[6–10] a U.S. Department of Energy analysis indicates that solar panels will need >30 yr service lifetimes with year-over-year degradation rates of less than 0.5% for a panel to reach \$0.03/kWh levelized cost of energy (assuming a 20% total-area efficiency and a module cost of \$0.19/W_p).[11] Testing the stability of any technology on multi-decade timescales is impractical. Therefore, warranties backing the long-term performance of HP-based commercial products will necessarily rely on predictions of service lifetime. While accelerated aging tests like the IEC 61215 standard (which includes testing the drop in performance after the panel is held at 85 °C and 85% RH for 1,000 hrs)[12] have been used to estimate service lifetime and provide performance guarantees,[7,8] these tests have only been validated for silicon and thin film based PV technologies like CdTe.[13–15] Unlike in Si or CdTe, HPs degrade due to chemical reactions of the semiconductor with water, oxygen, and photoexcited electrons,[6,16–20] and there exists a strong correlation between decay of optoelectronic properties such as carrier diffusion length and material transformation rate.[21,22] In oxygen and light, a photooxidation-induced degradation of $MAPbI_3$ has been reported previously[19,23,24] and is widely believed to occur via a mechanism that involves superoxide radical ($O_2^{\bullet -}$) generated by photoexcited electrons in the conduction band of $MAPbI_3$ to yield the overall reaction:[18–20,23,24]

$$4CH_3NH_3PbI_3 + O_2 + h\nu \rightarrow 4PbI_2 + 4CH_3NH_2 + 2H_2O + 2I_2 \quad \textbf{(1)}$$

Others have disputed the generation of water in this process, citing instead the overall reaction (note that PbI_2 and I_2 are not directly reported in this mechanism, but necessarily must be formed as stated to maintain charge and species conservation through the reaction):[20,25]

$$CH_3NH_3PbI_3 + O_2 + h\nu \rightarrow CH_3NH_2 + O_2 + \frac{1}{2}H_2 + PbI_2 + \frac{1}{2}I_2 \quad \textbf{(2)}$$

In humid environments, attack by moisture is widely reported to be the primary mode of degradation in $MAPbI_3$ thin films,[16,17] with an expected degradation pathway of:

$$CH_3NH_3PbI_3 + H_2O \rightleftharpoons CH_3NH_3PbI_3 \cdot H_2O \quad \textbf{(3)}$$

$$4CH_3NH_3PbI_3 \cdot H_2O \rightleftharpoons (CH_3NH_3)_4PbI_6 \cdot 2H_2O + 3PbI_2 + 2H_2O \quad \textbf{(4)}$$

$$(CH_3NH_3)_4PbI_6 \cdot 2H_2O \rightarrow 4CH_3NH_2 + 4HI + PbI_2 + 2H_2O \quad \textbf{(5)}$$

Despite these proposed overall reactions, quantitative acceleration factors describing how increasing oxygen, humidity, or illumination levels impact HP material degradation rate are still unknown. Without knowledge of these functionalities, it is unlikely that service lifetime predictions derived from accelerated-aging tests will be accurate. Recent machine learning studies have emerged to in an attempt to fill this predictive gap,[21,26–28] with ML models identifying material decomposition rate (rate of increase of transmittance) as the most important quantitative predictors of diffusion length degradation over time (diffusion length T80).[21] However, if these models are to be predictive over multi-decade time scales, understanding of the physics that that govern $MAPbI_3$ degradation are required. Given the strong correlation between HP material degradation and that of their optoelectronic performance, accurate prediction of HP device lifetimes will greatly benefit from a fundamental understanding of the degradation mechanisms and the kinetics of each pathway of material degradation.

The degradation mechanisms and rates for commercial optoelectronics have been well-studied. For example, light-induced degradation due to the Staebler-Wronski effect in amorphous silicon has an understood mechanism and rate orders,[29] and the light-induced degradation in crystalline silicon PVs has been demonstrated to be due to oxidation of boron defects in the silicon lattice, with well-agreed upon activation energies and rate constants for both slow and fast boron deactivation processes.[14] Despite the importance of HP degradation reactions, a formal mechanism with rate orders and rate constants has not been reported. Some reports of effective rate constants and activation energies of perovskite degradation exist from fits to an Avrami model[30] based on the time-evolution of optical absorbance,[31] XRD patterns,[32–35] XPS peaks,[36] and AFM features of degrading HP films.[37] However, quantitative relationships between the rate of perovskite degradation and partial pressure of oxygen, the illumination intensity, and the partial pressure of water vapor are still unknown.

Here, we measure the kinetics of methylammonium lead iodide ($MAPbI_3$) perovskite transformation using changes in optical transmittance measured in-situ as a function of humidity, oxygen, illumination intensity, and temperature to construct a rate law equation. Transmittance is collected with an incident photon wavelength of 550 nm (~2.25 eV), which is above the bandgap of $MAPbI_3$ (1.6 eV) and below the bandgap of all reported solid degradation products, namely: PbI_2 (2.35 eV),[16,38] $CH_3NH_3PbI_3{\cdot}H_2O$ (3.1 eV),[31] $CH_3NH_3PbI_3{\cdot}2H_2O$ (3.9 eV),[39] and $PbO_{1-x}(OH)_{2x}$ (>2.5 eV).[40] Increases in transmittance are therefore interpreted as conversion of $MAPbI_3$ to degradation products. We identify and quantify two mechanisms of degradation: (a) dry photooxidation (DPO) process that occurs in the absence of vapor-phase water, and (b) a water-accelerated photooxidation (WPO). For each mode of degradation, we identify how varying environmental conditions impact the initial rate of $MAPbI_3$ degradation (r_{MAPI}) in both regimes, extracting activation energies and rate orders in humidity, oxygen, and light. The experimentally determined rate orders are highly suggestive of certain elementary steps in the mechanism, and we propose a detailed reaction mechanism for the degradation for $MAPbI_3$ in the presence of oxygen, light, and humidity that explains the functionality of the rate law. The derived detailed reaction mechanism suggests that H_2O accelerates the photooxidation process of $MAPbI_3$.

Results and Discussion

The degradation of $MAPbI_3$ was monitored *in-situ* under controlled environmental conditions by simultaneous measurement of transmittance and quantitative photoluminescence.[21,41] (see Fig. 1a). Environmental conditions are controlled using a small chamber with gas ports, a heater, and windows above and below the sample to admit incident and transmitted light. The optical transmittance ($\mathcal{T}$, ratio of the sum of direct and diffuse transmitted intensity divided by incident intensity) is measured using incident 550 $\pm$ 15 nm monochromatic light from an LED source and notch filter. Thus, increasing $\mathcal{T}$ at 550 nm indicates increased degradation of the $MAPbI_3$ film (E_g = 1.6 eV, 775 nm) into PbI_2 (E_g = 2.35 eV, 525 nm) and volatile byproducts.[6,21,31] Absolute values of transmittance of a $MAPbI_3$ film placed the environmental chamber (which in turn is affixed to a microscope stage) are difficult to obtain in situ. Measured transmittance values on the same sample may change significantly based on position and orientation of the $MAPbI_3$ film in the chamber, the alignment of the photodiode sensor (which must be repositioned after focusing each sample due to adjustment of the z-height of the microscope stage during experimental setup), stray light from the environment, and other uncontrolled factors. To minimize these effects, it is desirable to use the transmittance normalized by the initial transmittance, ($\mathcal{T}_t/\mathcal{T}_0 = I_t/I_0$). This is the measured data in the experiments.

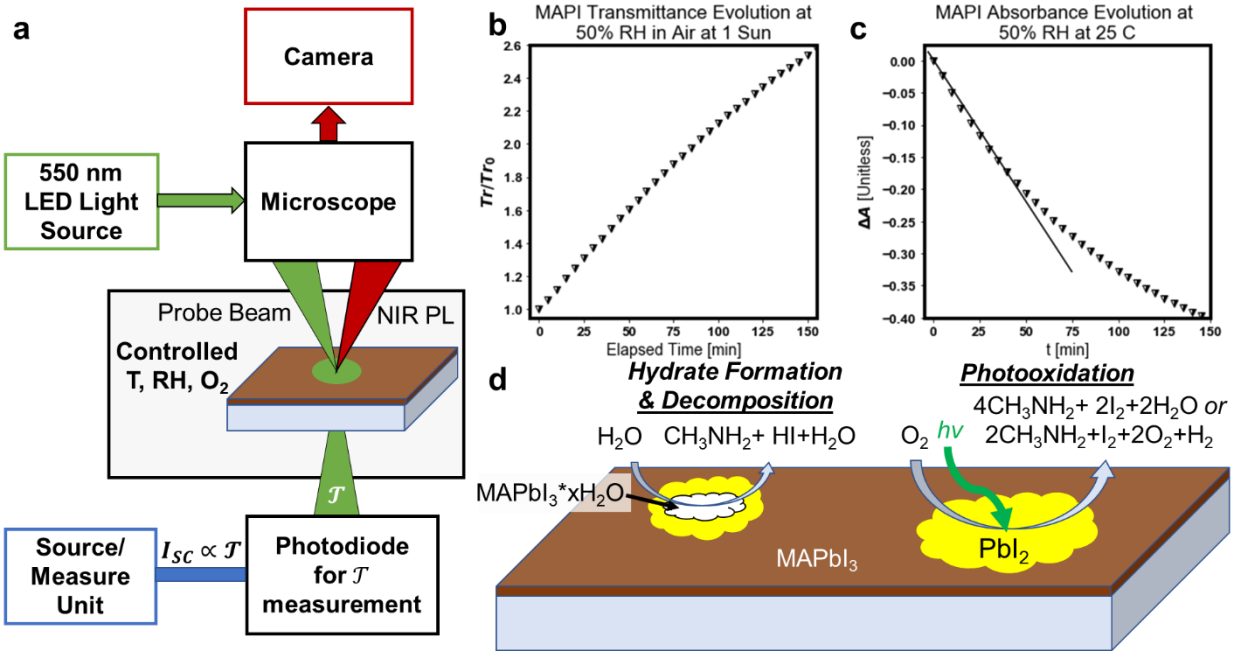

Figure 1. (a) Schematic of the experimental setup used to monitor perovskite decomposition under controlled environmental conditions. (b) Example of the evolution of transmittance for $MAPbI_3$ at 50% RH in air at 1 Sun effective illumination. (c) Change in absorbance over time, showing an initial linear region of a $MAPbI_3$ sample at 25 °C in 50% RH air under 1 Sun illumination. (d) Schematic detailing the most commonly reported degradation mechanisms of $MAPbI_3$ in literature: hydrate formation (requiring only water) and photooxidation (requiring only oxygen and light) with degradation products variously reported as either H_2 or H_2O.

For our purposes, the transmittance is important only in so far as it is used to calculate the absorbance, which can be related to the number of moles of perovskite (*N*). The Beer-Lambert law related the absorbance (A) to the conventionally defined material absorption coefficient α, $A = \alpha \cdot L \cdot log_{10}(e)$. As degradation occurs, perovskite is converted to higher bandgap materials and the effective absorption coefficient (above the perovskite bandgap but below the bandgap of the products) decreases. To account for this, we define an effective absorption coefficient, $\alpha = \alpha_0 \cdot (N/N_0)$ where α_0 is the absorption coefficient of pristine perovskite at the wavelength of the incident light (550 nm) and N_0 is the initial number of moles of $CH_3NH_3PbI_3$ in the beam path. Substituting in the effective absorption coefficient and taking the derivative with respect to time yields, $dA/dt = \alpha_0 \cdot (1/N_0) \cdot L \cdot log_{10}(e) \cdot dN/dt$. In the early stages of degradation, the change in absorbance evolves linearly with time (Fig. 1c) and is relatively independent of film thickness below 500 nm (Fig. S2). This suggests that the degradation reaction is dominated by surface reactions and is effectively zeroth order with respect to $MAPbI_3$ (see section 3 in Supporting Information). Thus, the rate of disappearance of $MAPbI_3$ is defined as negative the rate of change of moles of $MAPbI_3$ per unit area (W) of the illuminated film, $r_{MAPI} = -(1/W) \cdot dN/dt$. Plugging in the relation above between dA/dt and dN/dt and using $N_0/(W \cdot L) = \rho/M$, where ρ is the density of pristine perovskite and M is the formula weight, the equation for the rate of disappearance of perovskite in terms of absorbance is:

$$r_{MAPI} = -\frac{1}{W}\frac{dN}{dt} = -\frac{\rho}{M \cdot log_{10}(e) \cdot \alpha_0}\frac{dA}{dt} \quad \textbf{(6)}$$

When reflectance is negligible, the absorbance may be calculated from the transmittance, $A = -log_{10}(\mathcal{T})$. In the case where reflectance (both specular and diffuse) is not negligible but is dominated by the front interface reflectivity, the absorbance becomes $A = -log_{10}(\mathcal{T}/(1-R))$. Conveniently, the difference between the absorbance at time *t* minus the initial absorbance, ΔA, can be calculated from the directly measured transmittance normalized to time-zero values ($\mathcal{T}_t/\mathcal{T}_0$):

$$\Delta A = A_t - A_0 = -log_{10}\left(\frac{\mathcal{T}_t}{1-R_t}\right) - \left(-log_{10}\left(\frac{\mathcal{T}_o}{1-R_o}\right)\right) \quad \textbf{(7)}$$

$$\Delta A = -log_{10}\left(\frac{\mathcal{T}_t}{\mathcal{T}_0}\right) - log_{10}\left(\frac{1-R_o}{1-R_t}\right) \quad \textbf{(8)}$$

If changes in reflectance due to interference effects are small enough relative to changes in transmittance (which is the case during the early stages of degradation) then $(1-R_o)/(1-R_t)$ approaches 1 and thus the second term approaches zero, yielding:

$$\Delta A \approx -log_{10}\left(\frac{\mathcal{T}_t}{\mathcal{T}_0}\right) = -log_{10}\left(\frac{I_t}{I_0}\right) \quad \textbf{(9)}$$

Also, $d(\Delta A)/dt = dA/dt$. The reflectance does change some with time, and we calculate the error in the rate of reaction associated with neglecting the changes in reflectance (see section 2 and Fig. S1 of the Supporting Information). For measurement at 550 nm, the error is about 1%. Depending on how the incident wavelength aligns with the maxima or minima of the reflectance (which depends on film thickness), the error can be as large as 28%, which would be the case if we measured our films with 630 nm incident light (see Fig. S1). Given that the film thickness is effectively constant in the data set, 260 nm ± 10 nm, determined from profilometry, the error systemic error is small. Further, given that the differences in the rate of reaction presented below

span 3 orders of magnitude, the error associated with neglecting changes in reflectance does not affect any of the conclusions below.

The rate of change of absorbance encodes the dynamics of the $MAPbI_3$ degradation reaction and is a function of (at least) temperature, humidity, oxygen, and illumination intensity. Note that other factors may affect the rate as well like grain size and the concentration of point defects. Smaller grain sizes increase the grain boundary surface area and should increase the observed rate. With regard to defects, iodide vacancies in particular have been shown to facilitate superoxide formation and should also increase the observed rate.[42] The initial rate of degradation was determined using linear fits of the change in absorbance and eq. 6 at a variety of environmental conditions (Fig 2a-d and Table 1), both in the dark and under 1 Sun illumination (which here for a 1.6 eV bandgap material is approximated by continuous illumination with 1.59×10^{21} above-bandgap-photons/$m^2 \cdot s$). The initial rates reveal that photo-induced degradation in the presence of oxygen is faster than any process without oxygen (dry thermal or humid thermal under illumination or in the dark) by more than an order of magnitude at both 25 ^oC and 85 ^oC. Dry oxygen and humid oxygen pathways are approximately equal at 85 ^oC, while the humid-oxygen pathway dominates at 25 ^oC by an order of magnitude. Importantly, the data show that in the absence of oxygen, humidity-only degradation is much slower relative to degradation in the presence of oxygen. Similarly, other reported degradation pathways that contribute to $MAPbI_3$ degradation are much also much slower than photooxidation processes. Thermal degradation[43] at 85 ^oC is three orders of magnitude slower than photooxidative degradation. C-N bond cleavage in methylammonium due to blue light (λ>410 nm) exposure has also been reported to contribute to $MAPbI_3$ degradation.[20,25] However, exposure to 1 sun equivalent of 395 nm light results in degradation rates below 1×10^{-10} mol/m^2s, again over three orders of magnitude slower than photooxidation processes. A summary of relative rates of degradation is shown in Table 1.

The apparent activation energy of photooxidation is calculated to be 0.47 eV in dry air and 0.08 eV in 50% RH air. As a result of these dramatically different activation energies, photooxidation rates in the presence and absence of humidity differ significantly depending on the temperature, and dry photooxidation proceeds at a rate that is over an order of magnitude slower than humidity-assisted photooxidation at 25 ^oC (Table 1). Together these results indicate that water and oxygen synergistically accelerate $MAPbI_3$ degradation. It is sometimes assumed that the observed increased degradation rate in the presence of both oxygen and water is due to the additive effects of humidity only (degradation via hydrate formation) and dry photooxidative pathways.[44] However, degradation rates in humidity without oxygen and in oxygen without humidity both proceed at over an order of magnitude slower pace than $MAPbI_3$ degradation rate in the presence of both humidity and oxygen. These data thus point to water acting as an accelerant (technically not a catalyst since water is consumed as an intermediate and then generated as a product) for photooxidation of $MAPbI_3$, rather than contributing to degradation via a parallel hydration pathway.

This is consistent with some speculation in literature. Aristidou et. al. have reported that increasing water concentration in a toluene solution submerging a $MAPbI_3$ film increases superoxide yield, and by extension, degradation rate.[23] They speculate that this increased yield is due to increasing proton concentration at the $MAPbI_3$ surface, which makes superoxide protonation more favorable.[23] Figure 2 supports this idea, demonstrating that the presence of humidity dramatically increases photooxidation rate, even in the vapor phase. Furthermore, data in Figure 2 demonstrates that the presence of acidic water protons do not merely provide additional

protons to contribute to reaction, but that water creates a lower energy barrier for the overall reaction, indicating this protonation is likely the significant rate-limiting process in overall $MAPbI_3$ decomposition. Others still have shown using molecular simulations that water adsorption can impact energy levels of adsorbed oxygen,[45] especially in the limit of excess hole concentration in the $MAPbI_3$ surface.[46] This is consistent with the observation in Figure 2 and Table 1 of humidity-accelerated photooxidation pathways.

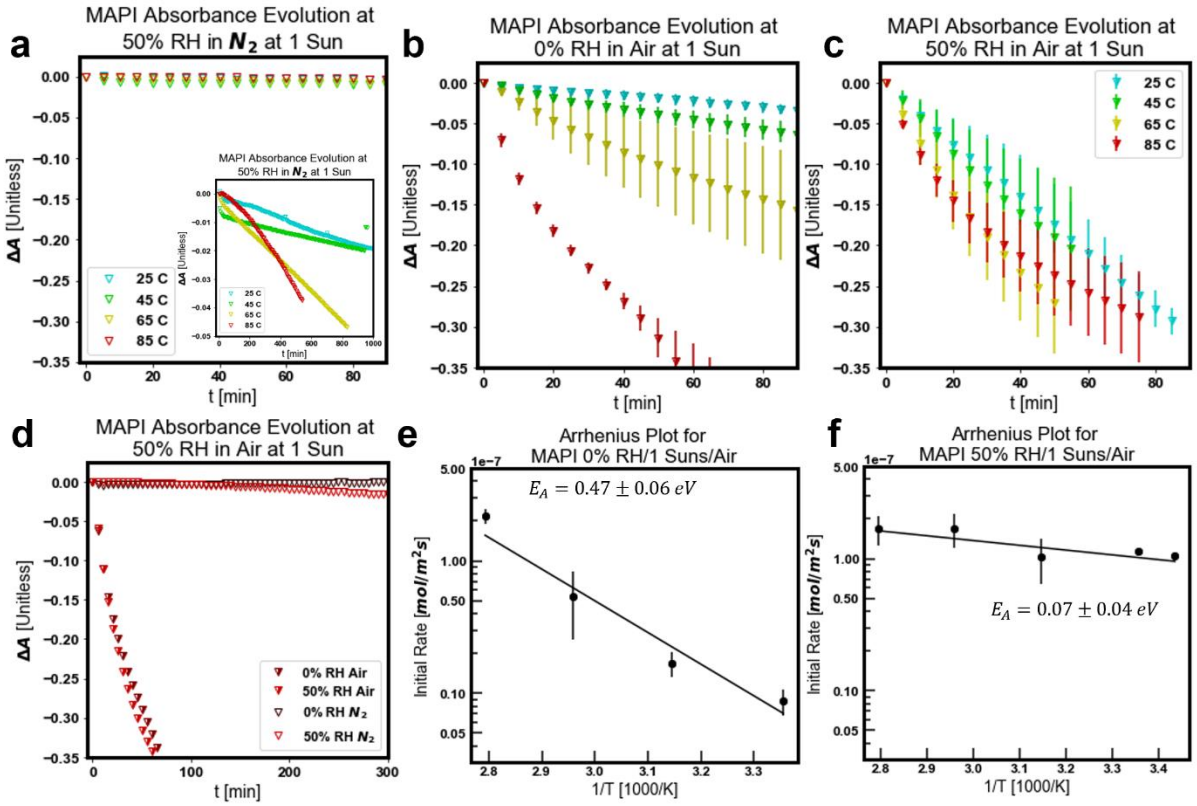

Figure 2. Absorbance evolution of $MAPbI_3$ thin films vs time aged at 25, 45, 65, and 85 °C under 1 sun excitation in (a) 50% RH N_2, (b) 0% RH air ("dry air"), and (c) 50% RH air ("humid air"). (d) Degradation proceeds rapidly in both humid and dry air, but slowly in humid and dry nitrogen, indicating that the primary modes of $MAPbI_3$ degradation are photooxidation and humidity-accelerated photooxidation. Arrhenius plots of initial $MAPbI_3$ degradation in (e) dry and (f) humid air conditions.

Table 1. Upper bounds on degradation rates of different degradation processes at 25 and 85 °C. While the initial degradation rate for photooxidation at 85 °C in both dry and humid air is ~10^{-7} mol/m^2/s, degradation in humid nitrogen is 2 orders of magnitude lower, and degradation due to thermal-only and light-only degradation processes in inert environments is over 3 orders of magnitude slower than photooxidative processes. The full table showing degradation in corresponding dark conditions is in Supporting Information as Table S1. In most cases, degradation in the dark is dominated by the periods during which the sample is illuminated by the probe beam when collecting optical measurements, as seen by the acceleration of degradation when the measurement frequency is increased (see §4 of Supporting Information). Where repeat runs were performed, the uncertainty is represented by the standard deviation ($\pm\sigma$). The random error associated with sample-to-sample variation in the degradation rate is <25% in all cases reported here, and is of similar scale to the upper bound on the systematic error associated with neglecting reflectance effects (see §2 of Supporting Information and Fig. S1). At a probe wavelength of 550 nm, however, the systematic error is much lower (~1%) and is therefore generally insignificant relative to sample-to-sample variation. ****** See note at the end of the abstract.

Degradation Conditions	**25 ºC with 1 Sun [mol/(m^2·s)]**	**85 ºC with 1 Sun [mol/(m^2·s)]**
Heat Only (0% O_2, 0% RH)	less than 10^{-10}	less than 10^{-10}
Humid N_2 (0% O_2, 50% RH)	5×10^{-10}	2×10^{-9}
Dry Air (21% O_2, 0% RH)	$8.7 \pm 1.9 \times 10^{-9}$ ******	$2.2 \pm 0.3 \times 10^{-7}$
Humid Air (21% O_2, 50% RH)	$1.1 \pm 0.04 \times 10^{-7}$	$1.7 \pm 0.4 \times 10^{-7}$

Having identified primary degradation modes, rate orders in humid and dry air conditions are determined by establishing a baseline set of conditions for dry photooxidation (25 ºC, 0% RH, 21 kPa O_2, 1 sun illumination) and humid photooxidation (25 ºC, 50% RH, 21 kPa O_2, 1 sun illumination) degradation modes and measuring the response of sample absorbance to varying oxygen content, illumination intensity, and humidity levels. Results are shown in Figure 3. In humid air conditions, rate of $MAPbI_3$ degradation (r_{MAPI}) proceeds with rate orders of 1.3 $\pm$ 0.3 (i.e., approximately first order) with respect to the partial pressure of water in the gas phase, 0.28 $\pm$ 0.05 with respect to the partial pressure of oxygen, and 0.25 $\pm$ 0.03 with respect to the illumination intensity. In dry air, r_{MAPI} proceeds with rate orders of 0.11 $\pm$ 0.15 with respect to oxygen (approximately zeroth order), and 0.7 with respect to illumination intensity. This number is consistent with the power-law dependence on the illumination intensity in $MAPbI_3$ thin films. In particular, photoconductivity experiments[41,47] have shown $n \propto N_{suns}^{0.4}$ and $N_{suns}^{0.73}$, respectively. These results are consistent with data from these samples, which show $n \propto N_{suns}^{0.67}$ (Figure S5) (see §5 in Supporting Information). Therefore, we conclude that a rate order of 0.71 with respect to illumination intensity is equivalent to first order kinetics in excess carrier concentration. The observed rate orders are determined by the mechanism, and thus the experimentally determined rate orders constrain the possible reaction mechanisms. However, for multi-step reactions, observed rate orders may vary depending on the concentrations of various species. If the elementary steps are known (or can be guessed by physicochemical reasoning) and the rate of one step determines the rate of the overall reaction (while all other steps are in quasi-equilibrium), then an approximate rate equation can be derived. While the concept of a rate determining step (RDS) is often debated[48,49] with compelling reasons to develop more general approaches, the approach has tremendous utility in deriving the functional form of approximate rate equations for many multi-step reactions.[50,51]

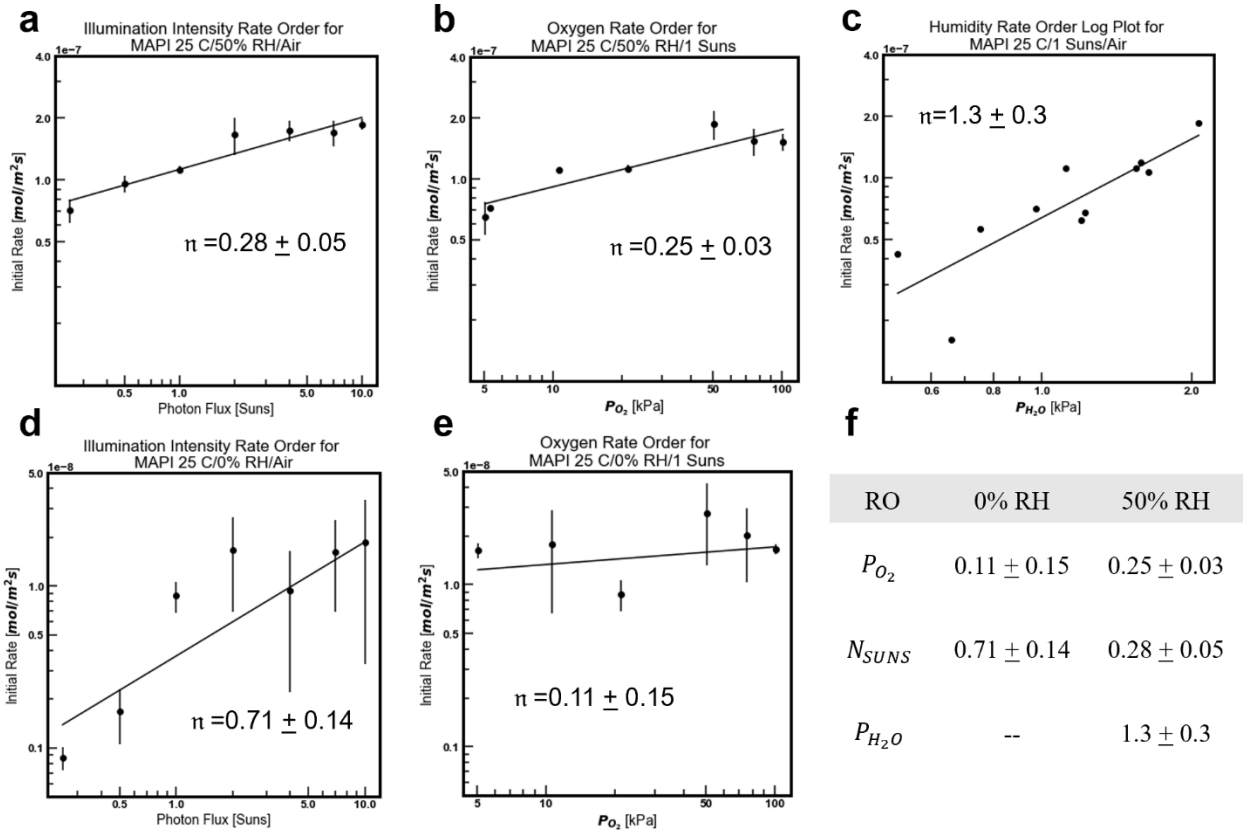

RO	0% RH	50% RH
P_{O_2}	0.11 ± 0.15	0.25 ± 0.03
N_{SUNS}	0.71 ± 0.14	0.28 ± 0.05
P_{H_2O}	--	1.3 ± 0.3

Figure 3. Effective rate orders based on initial degradation rates for (a,d) illumination, (b,e) oxygen, and (c) water for $MAPbI_3$ films at 25 °C in (a-c) humid and (d,e) dry atmospheres. (f) A summary table of effective rate orders in oxygen, illumination, and moisture.

Considering possible pathways for photooxidation (without water), previously it has been reported that neutral oxygen adsorbs on the surface of $MAPbI_3$ (preferably in/on iodide vacancies)[19,45] which then gets reduced by photoexcited electrons from the conduction band of $MAPbI_3$ to form superoxide radical, ($O_2^{\bullet-}$).[24,40,45] Here, we will develop a kinetic expression using [*] to indicate an unoccupied absorption site. Further, it has been reported[18,20,52] that superoxide radicals abstract a proton from the methylammonium cation ($CH_3NH_3^+$). Such a mechanism would yield an adsorbed hydroperoxyl radical ($O_2^{\bullet-*} + H^+ \rightarrow HO_2^{\bullet*}$).[53] Once the peroxyl radical is present, other reactive oxygen species (ROS) are possible, including but not limited to:

$$2\,HO_2^{\bullet} \rightleftharpoons H_2O_2 + O_2 \quad \textbf{(10)}$$

$$H_2O_2 \rightleftharpoons 2HO^{\bullet} \quad \textbf{(11)}$$

$$H_2O_2 + e^- \rightleftharpoons HO^{\bullet} + HO^- \quad \textbf{(12)}$$

Each of the reactive oxygen species ($O_2^{\bullet-}, HO_2^{\bullet}, H_2O_2, HO^{\bullet}, HO^-$) may react with methylammonium, abstracting either a proton or a neutral hydrogen. One ***plausible*** complete dry photo-oxidation pathway is shown in scheme 1.

Scheme 1. One Plausible Dry photo-oxidation Pathway. Primary degradation mechanism of $MAPbI_3$ in the absence of water but in the presence of oxygen, above bandgap incident photons, and surface adsorption sites [*].

$$2h\nu \rightarrow 2e^- + 2h^+ \qquad \textit{(step D1)}$$

$$O_2 + [*] \rightleftharpoons O_2^* \qquad \textit{(step D2)}$$

$$O_2^* + e^- \rightleftharpoons O_2^{\bullet -*} \qquad \textit{(step D3)}$$

$$CH_3NH_3PbI_3 + O_2^{\bullet -*} \rightarrow HO_2^{\bullet *} + PbI_2 + CH_3NH_2 + I^- \qquad \textit{(step D4)}$$

$$CH_3NH_3PbI_3 + HO_2^{\bullet *} \rightarrow H_2O_2^* + PbI_2 + CH_3NH_2 + I^{\bullet} \qquad \textit{(step D5)}$$

$$H_2O_2^* + e^- + [*] \rightleftharpoons HO^{-*} + HO^{\bullet *} \qquad \textit{(step D6)}$$

$$CH_3NH_3PbI_3 + HO^{\bullet *} \rightarrow H_2O^* + PbI_2 + CH_3NH_2 + I^{\bullet} \qquad \textit{(step D7)}$$

$$CH_3NH_3PbI_3 + HO^- \rightarrow H_2O^* + PbI_2 + CH_3NH_2 + I^- \qquad \textit{(step D8)}$$

$$2h^+ + 2CH_3NH_3PbI_3 \rightleftharpoons 2CH_3NH_3PbI_2^+ + 2[*] + 2I^{\bullet} \qquad \textit{(step D9)}$$

$$2CH_3NH_3PbI_2^+ + 2[*] + 2I^- \rightleftharpoons 2CH_3NH_3PbI_3 \qquad \textit{(step D10)}$$

$$4I^{\bullet} \rightarrow 2I_2 \qquad \textit{(step D11)}$$

There are many ways that the reaction in scheme 1 can happen from step D5 onwards, depending on the relative rates of formation of different ROS and the specific products. However, most variations result in the same rate law that is zeroth order in oxygen and first order in concentration of electrons, provided that step 4 (proton abstraction from methylammonium by superoxide) is the rate determining step. The resulting rate equation for dry photo-oxidation (DPO) degradation of $MAPbI_3$ is (see §6 of Supporting Information for the derivation):

$$r_{DPO} = -k_{DPO} n \qquad \textbf{(13)}$$

where $k_{DPO} = k_{0,DPO}\, e^{-E_{a,DPO}/k_B T}$. The measured rate of dry photo-oxidation is compared to the derived rate law in Figure 5. It is important to note that in these experiments dry air is swept over the sample, and thus any water, iodine (see §8 of Supporting Information), or other volatile products) are removed from the system. In a device architecture, especially encapsulated architectures, these products will build-up. ***This could be especially problematic with water since the water-accelerated photo-oxidation is much faster than dry photo-oxidation, and over time an encapsulated film may transition from dry photo-oxidation to water-accelerated photo-oxidation***. Further, it suggests that ***oxygen barrier properties*** might be the most critical packaging perovskite solar cells for long-term stability.

In the presence of water, many additional pathways are possible to form ROS. One reaction that is particularly noteworthy is: $O_2^{\bullet -} + H_2O \leftrightarrows HO_2^{\bullet} + HO^-$. The rapid reaction between superoxide radical and H_2O is well-known.[53,54] Here, we hypothesize that superoxide more rapidly reacts with adsorbed water than methylammonium, shifting the rate determining step, and thus significantly altering the rate equation. One ***plausible*** water-mediated photo-oxidation pathway is shown in Scheme 2.

Scheme 2. One Plausible Water-Accelerated Photo-oxidation Pathway. Primary degradation mechanism of $MAPbI_3$ in the presence of water, oxygen, above bandgap incident photons, and surface adsorption sites [*].

$$2h\nu \rightarrow 2e^- + 2h^+ \qquad \textit{(step H1)}$$

$$O_2 + [*] \rightleftharpoons O_2^* \qquad \textit{(step H2)}$$

$$H_2O + [*] \rightleftharpoons H_2O^* \qquad \textit{(step H3)}$$

$$O_2^* + e^- \rightleftharpoons O_2^{*\bullet -} \qquad \textit{(step H4)}$$

$$O_2^{\bullet -*} + H_2O^* \rightarrow HO_2^{\bullet *} + HO^{-*} \qquad \textit{(step H5)}$$

$$CH_3NH_3PbI_3 + HO_2^{\bullet *} \rightarrow H_2O_2^* + PbI_2 + CH_3NH_2 + I^\bullet \qquad \textit{(step H6)}$$

$$H_2O_2^* + e^- + [*] \rightleftharpoons HO^{-*} + HO^{\bullet *} \qquad \textit{(step H7)}$$

$$CH_3NH_3PbI_3 + HO^{\bullet *} \rightarrow H_2O^* + PbI_2 + CH_3NH_2 + I^\bullet \qquad \textit{(step H8)}$$

$$2CH_3NH_3PbI_3 + 2HO^- \rightarrow 2H_2O^* + 2PbI_2 + 2CH_3NH_2 + 2I^- \qquad \textit{(step H9)}$$

$$2h^+ + 2CH_3NH_3PbI_3 \rightleftharpoons 2CH_3NH_3PbI_2^+ + 2[*] + 2I^\bullet \qquad \textit{(step H10)}$$

$$2CH_3NH_3PbI_2^+ + 2[*] + 2I^- \rightleftharpoons 2CH_3NH_3PbI_3 \qquad \textit{(step H11)}$$

$$4I^\bullet \rightarrow 2I_2 \qquad \textit{(step H12)}$$

Since water is regenerated in this reaction, it has a catalyst-like effect. An expression for the rate of $MAPbI_3$ degradation in humid air is determined by assuming: (i) the rate determining step in Scheme 2 is step H5—deprotonation of water by superoxide to form hydroxide and hydroperoxyl radicals—and (ii) the fractional surface coverage of water is small in the range of humidity levels studied (i.e. $K_3P_{H_2O} \ll 1 + K_2P_{O_2}(1 + K_4n)$, and we are hence in the quasilinear regime of the Langmuir isotherm of water such that $\theta_{H_2O} \approx K_{eq,H3}P_{H_2O}$).

With these assumptions, r_{WPO} simplifies to (see §7 of Supporting Information for the derivation):

$$r_{WPO} = -k_{WPO}\frac{P_{H_2O}P_{O_2}n}{\left(1 + K_2P_{O_2}(1 + K_4n)\right)^2} \qquad \textbf{(14)}$$

where $k_{WPO} = k_{0,WPO}\, e^{-E_{a,WPO}/k_BT}$. In order to assess the validity of the functional form of the derived rate equation, the measured rate data are plotted as functions of oxygen concentration and photon flux and fitted to eq. 14 in Figure 4, along with simple power law relations (the functional forms fit in Figure 3). Figure 4 demonstrates that when varying illumination intensity in air, as well as from varying oxygen content under 1 sun illumination intensity, degradation rates more closely match the functional forms expressed in eq. 14 than simple rate law dependence.

Some research groups have disputed the commonly held consensus that water is produced as a byproduct in the dry photooxidation reaction.[20,25] They claim instead a mechanism where $2HO_2^\cdot$ species react once generated to form O_2 + H_2 instead of water vapor. This possibility is

explored in §6 of Supporting Information. Due to the rate limiting step in both mechanisms being shared—namely, that proton abstraction by superoxide is rate-limiting—both mechanisms yield the same rate expression for r_{DPO} and r_{WPO}. Similarly, presence of excess holes due to photogeneration and subsequent reaction of photoexcited electrons may trigger generation of iodide vacancies in $MAPbI_3$.[42] As iodide vacancies are the primary adsorption sites for both water vapor and oxygen, this can act as a generation reaction of new adsorption sites.[19,42,45] However, due to the mismatch in time scales between vacancy generation from holes and material degradation,[42] as well as the presence of many other adsorption sites for degradation,[45,55] the assumption that total adsorption site density is constant remains valid on these early timescales, leading to the same rate expressions for r_{DPO} and r_{WPO} (see (see §8 of Supporting Information for more details).

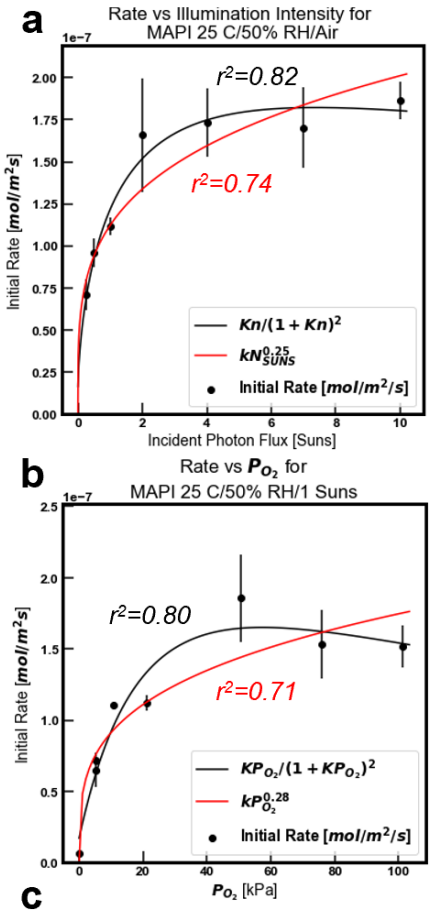

c

$r \propto f(X)$	0% RH	50% RH
$f(P_{O_2})$	1	$\frac{KP_{O_2}}{(1+KP_{O_2})^2}$
$f(n)$	n	$\frac{Kn}{(1+Kn)^2}$
$f(P_{H_2O})$	--	P_{H_2O}

Figure 4. (a) Rate of $MAPbI_3$ degradation vs incident photon flux in 25 °C air at 50% RH. Assuming the rate order of N_{SUNS} in dry air is equal to the power law dependence between N_{SUNS} and electron concentration (and consequently a_e),[41,47] we see that rate constant data in humid air is better fit to $kn/(1+kn)^2$, the derived expression relating rate and excess electron concentration, compared to a simple power law. (b) Rate of $MAPbI_3$ degradation vs partial pressure of oxygen P_{O_2} at 25 °C in 50% RH atmospheres under 1 sun illumination. As in (a), data are better fit to the derived functionality relating rate and oxygen pressure, $kP_{O_2}/(1+kP_{O_2})^2$, relative to a simple rate law fit. (c) A summary table of the functional forms of initial rate r_{MAPI} versus oxygen, moisture, and electron concentrations.

Table 2. Fit parameters for the parity plot in Figure 5. Partial pressures of oxygen and moisture are expressed in kPa, temperature in K, and incident above-bandgap-photon-flux I_{in} in photons·m^{-2}·s^{-1}. Boltzmann's constant is expressed as 8.617×10^{-5} eV/K, and E_{WPO} and E_{DPO} are the activation energies for the water-assisted and dry photooxidation pathways. The fit parameter c is the y-intercept of the fit rate expression, representing the sum rate of all minority degradation pathways. ** See note at end of abstract. Also, the parameter c is lower in the new ultra-dry dataset, as trace water was contributing to background rates.

Equation	
$r = k_{WPO} \exp\left(-\frac{E_{WPO}}{k_B T}\right) \frac{P_{O_2} P_{H_2O} I_{in}^{0.7}}{\left(1 + K_2 P_{O_2}(1 + K_4 I_{in}^{0.7})\right)^2} + k_{DPO} \exp\left(-\frac{E_{DPO}}{k_B T}\right) I_{in}^{0.7} + c$	
Parameter	Fit Value
k_{WPO}	$1.44 \times 10^{-23} \frac{mol}{m^2\, s\, kPa^2} \left(\frac{photons}{m^2 \cdot s}\right)^{-0.7}$
K_2	$6.9 \times 10^{-3}\ kPa^{-1}$
K_4	$3.98 \times 10^{-15} \left(\frac{photons}{m^2 \cdot s}\right)^{-0.7}$
k_{DPO}	$2.18 \times 10^{-24} \frac{mol}{m^2 \cdot s} \left(\frac{photons}{m^2 \cdot s}\right)^{-0.7}$
c	$1.12 \times 10^{-8} \frac{mol}{m^2 s}$

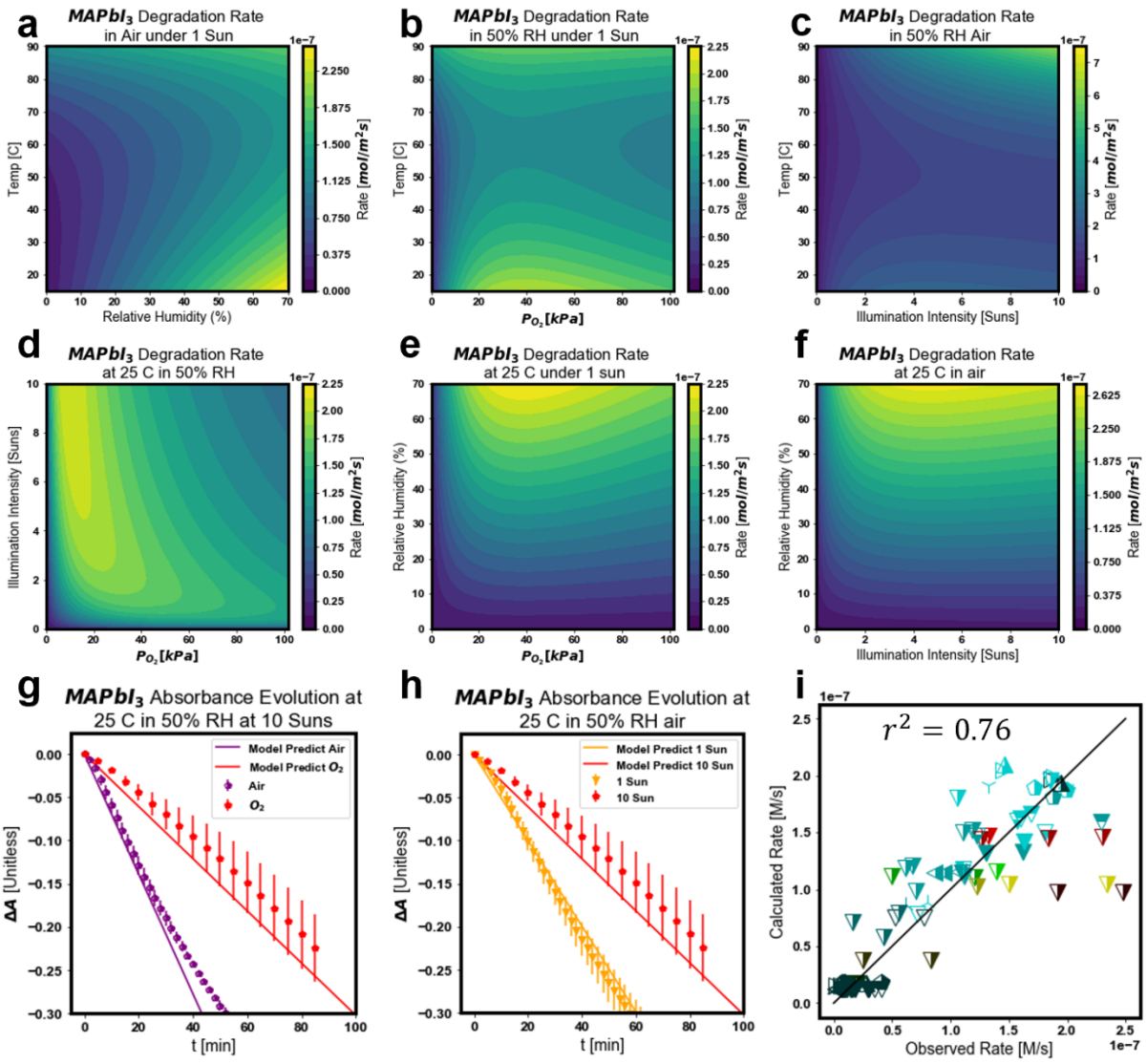

Figure 5. (a-f) Contour maps of $r_{MAPI} = r_{DPO} + r_{WPO}$ showing the functionality of the calculated rate expressions. Mechanistic crossover from DPO-dominant to WPO-dominant degradation is accounted for in Supporting Information. (g-h) Degradation of $MAPbI_3$ in 10 suns in pure O_2, validating the model prediction that humid air degradation occurs more slowly in increasing levels of (g) oxygen and (h) illumination intensity. Note data collected in 10 suns in O_2 was not used to fit the model; therefore, this result is validation of the functional form of r_{WPO} in extrapolated environmental conditions. (i) Parity plot comparing observed degradation rate against the sum of the humid and dry photooxidation rate expressions calculated based on rate order data. A good fit is achieved, with an r^2 of 0.76. ** See note at end of abstract.

The rate expressions in eq. 13-14 provide surprising implications for HP stability and accelerated aging of perovskite thin films. Contour plots of the prediction of total degradation rate $r = r_{DPO} + r_{WPO}$ are shown in Figure 5. Note that in humid air, observed degradation rates are the sum of r_{DPO} and r_{WPO}. At room temperature, r_{DPO} proceeds over an order of magnitude more slowly than r_{WPO}. However, at elevated temperature, r_{DPO} and r_{WPO} have similar characteristic

degradation rates. Therefore, prediction of humid-air degradation at high temperatures required calculation of degradation rates solely attributable to humidity-assisted photooxidation by $r_{WPO} = r_{MAPI} - r_{DPO}$.

One especially counter-intuitive conclusion of the functional form of r_{WPO} is that above critical values, increasing oxygen content and illumination intensity *decreases* degradation rate of $MAPbI_3$ (Figure 5d). To validate this conclusion, $MAPbI_3$ degradation was measured at 25 ^oC 50% RH O_2 under 10 suns illumination intensity. Note that r_{WPO} rate constants and functionalities were calculated from degradation experiments under 1 sun with changing oxygen pressure and in air with changing illumination intensity. Therefore, 10 suns in pure O_2 is an extrapolated environmental condition set relative to data used to fit the r_{WPO} equation. Nonetheless, degradation data collected in these conditions confirms the conclusions of the model (Figure 5g-h): degradation rates under high levels of oxygen *and* illumination stress are much slower than degradation rates under high levels of oxygen *or* illumination stress.

The mechanism and functional forms of r_{DPO} and r_{WPO} have significant implications for commercialization of halide perovskite technologies, particularly for stability validation and accelerated aging test protocols. The functional form of the rate law in humidity and resultant decelerating degradation rate indicate that caution should be used in interpreting convention stability test. ***High-temperature accelerated aging tests may be problematic***, as degradation at high temperatures (~85 ^oC) is dominated by the dry-photooxidation pathway, while degradation at 25 ^oC is dominated by the water accelerated photooxidation process. The contour plots, particularly Fig. 5d, suggests that ***accelerated testing at 6 Suns in humid air at 25 °C may be useful***. However, going to high oxygen concentration at any illumination is likely a bad idea since oxygen starts to out compete water for surface adsorption sites, decreasing the overall rate.

Furthermore, results from this work have implications for packaging and encapsulation of halide perovskite optoelectronics. Encapsulation materials—and even in some cases hole transporting materials—are specifically designed for hydrophobicity, with the belief that water alone is the primary cause for HP device degradation. However, results of this work demonstrate that ***oxygen ingress should likely be the most important process to inhibit.*** Unfortunately, flexible encapsulant layers have traditionally been unable to effectively block oxygen as effectively as moisture. While water-repellent barrier layers may still arrest room-temperature degradation at early times by eliminating the humidity-assisted photooxidation pathway at early times, these water-resistant layers may themselves probe problematic. It is widely proposed that water is a byproduct of the photooxidation reaction.[6,19,24] ***If water is produced during the photooxidation reaction, and then trapped on the perovskite surface by the hydrophobic barrier layer, residual water buildup near the halide perovskite surface may then set-off the water-accelerated photo-oxidation process over longer timescales, decreasing overall stability***. This conclusion may help explain recent results demonstrating increased PV stability in perovskites from hydrophilic passivation layers,[56] as these layers may help ***"getter" water generated from the photooxidation*** process away from the film, arresting the water-accelerated photooxidative pathway.

Conclusions

Fundamental kinetics governing the early-time degradation of halide perovskite $MAPbI_3$ were discovered in a unique automated data collection apparatus in a variety of controlled environmental conditions. Using absorbance at 550 nm as a probe of degradation extent, two

predominant modes of degradation were identified: (1) photooxidation due solely to the interaction of oxygen and photoexcited electrons (E_a=0.47 eV), and (2) humidity-accelerated photooxidation (E_a=0.08 eV). For each of these degradation modes, we identified rate orders in oxygen, humidity, and light intensity using rate constants extracted from linear fits of early-time absorbance evolution. Based on derived rate expressions, we propose a fundamental mechanism that details how oxygen degrades the $MAPbI_3$ lattice, including detail on the catalytic role of moisture in $MAPbI_3$ photooxidation.

Acknowledgments

The authors acknowledge financial support from the U.S. Department of Energy, Solar Energy Technology Office Grants DE-EE0008563 and DE-EE0009351, and the University of Washington Clean Energy Institute.

Declarations

The authors declare no competing financial interests

Supporting Information

Experimental details; supporting discussion and text; quantification of absorbance and reflectance as a function of degradation extent; thickness-dependent degradation rate; degradation rates in dark environments; how convective flow rate of $MAPbI_3$ impacts degradation rate; raw ΔA vs time data and linear fits of all data used in Figures 2-4, quantifying "pre-anneal" used to dry thin films before limiting case experiments; *J-V* curves of devices made from $MAPbI_3$ films and morphology; illumination intensity vs photoconductivity plot.

References

(1) Yoo, J. J.; Seo, G.; Chua, M. R.; Park, T. G.; Lu, Y.; Rotermund, F.; Kim, Y.-K.; Moon, C. S.; Jeon, N. J.; Correa-Baena, J.-P.; Bulović, V.; Shin, S. S.; Bawendi, M. G.; Seo, J. Efficient Perovskite Solar Cells via Improved Carrier Management. *Nature* **2021**, *590* (7847), 587–593. https://doi.org/10.1038/s41586-021-03285-w.

(2) Chang, N. L.; Ho-Baillie, A. W. Y.; Vak, D.; Gao, M.; Green, M. A.; Egan, R. J. Manufacturing Cost and Market Potential Analysis of Demonstrated Roll-to-Roll Perovskite Photovoltaic Cell Processes. *Sol. Energy Mater. Sol. Cells* **2018**, *174*, 314–324. https://doi.org/10.1016/j.solmat.2017.08.038.

(3) Mathews, I.; Sofia, S.; Ma, E.; Jean, J.; Laine, H. S.; Siah, S. C.; Buonassisi, T.; Peters, I. M. Economically Sustainable Growth of Perovskite Photovoltaics Manufacturing. *Joule* **2020**, *4* (4), 822–839. https://doi.org/10.1016/j.joule.2020.01.006.

(4) Mazzarella, L.; Lin, Y.; Kirner, S.; Morales-Vilches, A. B.; Korte, L.; Albrecht, S.; Crossland, E.; Stannowski, B.; Case, C.; Snaith, H. J.; Schlatmann, R. Infrared Light Management Using a Nanocrystalline Silicon Oxide Interlayer in Monolithic Perovskite/Silicon Heterojunction Tandem

Solar Cells with Efficiency above 25%. *Adv. Energy Mater.* **2019**, *9* (14), 1803241. https://doi.org/10.1002/aenm.201803241.

(5) Al-Ashouri, A.; Köhnen, E.; Li, B.; Magomedov, A.; Hempel, H.; Caprioglio, P.; Márquez, J. A.; Morales Vilches, A. B.; Kasparavicius, E.; Smith, J. A.; Phung, N.; Menzel, D.; Grischek, M.; Kegelmann, L.; Skroblin, D.; Gollwitzer, C.; Malinauskas, T.; Jošt, M.; Matič, G.; Rech, B.; Schlatmann, R.; Topič, M.; Korte, L.; Abate, A.; Stannowski, B.; Neher, D.; Stolterfoht, M.; Unold, T.; Getautis, V.; Albrecht, S. Monolithic Perovskite/Silicon Tandem Solar Cell with >29% Efficiency by Enhanced Hole Extraction. *Science* **2020**, *370* (6522), 1300–1309. https://doi.org/10.1126/science.abd4016.

(6) Dunfield, S. P.; Bliss, L.; Zhang, F.; Luther, J. M.; Zhu, K.; Hest, M. F. A. M.; Reese, M. O.; Berry, J. J. From Defects to Degradation: A Mechanistic Understanding of Degradation in Perovskite Solar Cell Devices and Modules. *Adv. Energy Mater.* **2020**, *10* (26), 1904054. https://doi.org/10.1002/aenm.201904054.

(7) Matsui, T.; Yamamoto, T.; Nishihara, T.; Morisawa, R.; Yokoyama, T.; Sekiguchi, T.; Negami, T. Compositional Engineering for Thermally Stable, Highly Efficient Perovskite Solar Cells Exceeding 20% Power Conversion Efficiency with 85 °C/85% 1000 h Stability. *Adv. Mater.* **2019**, *31* (10), 1806823. https://doi.org/10.1002/adma.201806823.

(8) Shi, L.; Bucknall, M. P.; Young, T. L.; Zhang, M.; Hu, L.; Bing, J.; Lee, D. S.; Kim, J.; Wu, T.; Takamure, N.; McKenzie, D. R.; Huang, S.; Green, M. A.; Ho-Baillie, A. W. Y. Gas Chromatography–Mass Spectrometry Analyses of Encapsulated Stable Perovskite Solar Cells. *Science* **2020**, *368* (6497), eaba2412. https://doi.org/10.1126/science.aba2412.

(9) Choi, K.; Lee, J.; Choi, H.; Kim, G.-W.; Kim, H. I.; Park, T. Heat Dissipation Effects on the Stability of Planar Perovskite Solar Cells. *Energy Environ. Sci.* **2020**, *13* (12), 5059–5067. https://doi.org/10.1039/D0EE02859B.

(10) Yang, N.; Zhu, C.; Chen, Y.; Zai, H.; Wang, C.; Wang, X.; Wang, H.; Ma, S.; Gao, Z.; Wang, X.; Hong, J.; Bai, Y.; Zhou, H.; Cui, B.-B.; Chen, Q. An *in Situ* Cross-Linked 1D/3D Perovskite Heterostructure Improves the Stability of Hybrid Perovskite Solar Cells for over 3000 h Operation. *Energy Environ. Sci.* **2020**, *13* (11), 4344–4352. https://doi.org/10.1039/D0EE01736A.

(11) US Department of Energy Solar Energy Technologies Office. *The Sunshot 2030 Goals: 3 Cent per Kilowatt Hour for PV and 5 Cent per Kilowatt Hour for Dispatchable CSP*; White Paper DOE/EE-1501; US Department of Energy, Office of Energy Efficiency and Renewable Energy, 2017.

(12) International Electrotechnical Commission. *IEC 61215-2:2021 RLV Redline Version. Terrestrial Photovoltaic Modules-Design Qualificiation and Type Approval*; Testing Standards IEC 61215-2:2021; International Electrotechnical Comission: Geneva, Switzerland, 2021.

(13) Jordan, D. C.; Kurtz, S. R. Photovoltaic Degradation Rates-an Analytical Review: Photovoltaic Degradation Rates. *Prog. Photovolt. Res. Appl.* **2013**, *21* (1), 12–29. https://doi.org/10.1002/pip.1182.

(14) Lindroos, J.; Savin, H. Review of Light-Induced Degradation in Crystalline Silicon Solar Cells. *Sol. Energy Mater. Sol. Cells* **2016**, *147*, 115–126. https://doi.org/10.1016/j.solmat.2015.11.047.

(15) Gretener, C.; Perrenoud, J.; Kranz, L.; Cheah, E.; Dietrich, M.; Buecheler, S.; Tiwari, A. N. New Perspective on the Performance Stability of CdTe Solar Cells. *Sol. Energy Mater. Sol. Cells* **2016**, *146*, 51–57. https://doi.org/10.1016/j.solmat.2015.11.017.

(16) Christians, J. A.; Miranda Herrera, P. A.; Kamat, P. V. Transformation of the Excited State and Photovoltaic Efficiency of $CH_3NH_3PbI_3$ Perovskite upon Controlled Exposure to Humidified Air. *J. Am. Chem. Soc.* **2015**, *137* (4), 1530–1538. https://doi.org/10.1021/ja511132a.

(17) Müller, C.; Glaser, T.; Plogmeyer, M.; Sendner, M.; Döring, S.; Bakulin, A. A.; Brzuska, C.; Scheer, R.; Pshenichnikov, M. S.; Kowalsky, W.; Pucci, A.; Lovrinčić, R. Water Infiltration in

Methylammonium Lead Iodide Perovskite: Fast and Inconspicuous. *Chem. Mater.* **2015**, *27* (22), 7835–7841. https://doi.org/10.1021/acs.chemmater.5b03883.

(18) Wei, J.; Wang, Q.; Huo, J.; Gao, F.; Gan, Z.; Zhao, Q.; Li, H. Mechanisms and Suppression of Photoinduced Degradation in Perovskite Solar Cells. *Adv. Energy Mater.* **2021**, *11* (3), 2002326. https://doi.org/10.1002/aenm.202002326.

(19) Aristidou, N.; Sanchez-Molina, I.; Chotchuangchutchaval, T.; Brown, M.; Martinez, L.; Rath, T.; Haque, S. A. The Role of Oxygen in the Degradation of Methylammonium Lead Trihalide Perovskite Photoactive Layers. *Angew. Chem.* **2015**, *127* (28), 8326–8330. https://doi.org/10.1002/ange.201503153.

(20) Nickel, N. H.; Lang, F.; Brus, V. V.; Shargaieva, O.; Rappich, J. Unraveling the Light-Induced Degradation Mechanisms of $CH_3NH_3PbI_3$ Perovskite Films. *Adv. Electron. Mater.* **2017**, *3* (12), 1700158. https://doi.org/10.1002/aelm.201700158.

(21) Stoddard, R. J.; Dunlap-Shohl, W. A.; Qiao, H.; Meng, Y.; Kau, W. F.; Hillhouse, H. W. Forecasting the Decay of Hybrid Perovskite Performance Using Optical Transmittance or Reflected Dark-Field Imaging. *ACS Energy Lett.* **2020**, *5* (3), 946–954. https://doi.org/10.1021/acsenergylett.0c00164.

(22) Lin, H.-J.; Cacovich, S.; Rebai, A.; Rousset, J.; Longeaud, C. Influence of Environment and Light-Stress on the Optoelectronic Properties of Triple-Cation Perovskite Thin Films. *ACS Appl. Mater. Interfaces* **2020**, *12* (17), 19495–19503. https://doi.org/10.1021/acsami.0c01732.

(23) Aristidou, N.; Eames, C.; Islam, M. S.; Haque, S. A. Insights into the Increased Degradation Rate of $CH_3NH_3PbI_3$ Solar Cells in Combined Water and O_2 Environments. *J. Mater. Chem. A* **2017**, *5* (48), 25469–25475. https://doi.org/10.1039/C7TA06841G.

(24) Aristidou, N.; Eames, C.; Sanchez-Molina, I.; Bu, X.; Kosco, J.; Islam, M. S.; Haque, S. A. Fast Oxygen Diffusion and Iodide Defects Mediate Oxygen-Induced Degradation of Perovskite Solar Cells. *Nat. Commun.* **2017**, *8* (1), 15218. https://doi.org/10.1038/ncomms15218.

(25) Rappich, J.; Lang, F.; Brus, V. V.; Shargaieva, O.; Dittrich, T.; Nickel, N. H. Light-Induced Defect Generation in $CH_3NH_3PbI_3$ Thin Films and Single Crystals. *Sol. RRL* **2020**, *4* (2), 1900216. https://doi.org/10.1002/solr.201900216.

(26) Sun, S.; Tiihonen, A.; Oviedo, F.; Liu, Z.; Thapa, J.; Zhao, Y.; Hartano, N. T. P.; Goyal, A.; Heumueller, T.; Batali, C.; Encinas, A.; Yoo, J. J.; Li, R.; Ren, Z.; Peters, I. M.; Brabec, C. J.; Bawendi, M. G.; Stevanovic, V.; Fisher III, J.; Buonassisi, T. A Data Fusion Approach to Optimize Compositional Stability of Organic-Inorganic Perovskite. *Matter* **2021**, *Early Access*. https://doi.org/doi.org/10.1016/j.matt.2021.01.008.

(27) Higgins, K.; Valleti, S. M.; Ziatdinov, M.; Kalinin, S. V.; Ahmadi, M. Chemical Robotics Enabled Exploration of Stability in Multicomponent Lead Halide Perovskites via Machine Learning. *ACS Energy Lett.* **2020**, *5* (11), 3426–3436. https://doi.org/10.1021/acsenergylett.0c01749.

(28) Hartono, N. T. P.; Thapa, J.; Tiihonen, A.; Oviedo, F.; Batali, C.; Yoo, J. J.; Liu, Z.; Li, R.; Marrón, D. F.; Bawendi, M. G.; Buonassisi, T.; Sun, S. How Machine Learning Can Help Select Capping Layers to Suppress Perovskite Degradation. *Nat. Commun.* **2020**, *11* (1), 4172. https://doi.org/10.1038/s41467-020-17945-4.

(29) Stutzmann, M.; Jackson, W. B.; Tsai, C. C. Kinetics of the Staebler–Wronski Effect in Hydrogenated Amorphous Silicon. *Appl. Phys. Lett.* **1984**, *45* (10), 1075–1077. https://doi.org/10.1063/1.95020.

(30) Avrami, M. Kinetics of Phase Change. I General Theory. *J. Chem. Phys.* **1939**, *7* (12), 1103–1112. https://doi.org/10.1063/1.1750380.

(31) Siegler, T. D.; Houck, D. W.; Cho, S. H.; Milliron, D. J.; Korgel, B. A. Bismuth Enhances the Stability of $CH_3NH_3PbI_3$ (MAPI) Perovskite under High Humidity. *J. Phys. Chem. C* **2019**, *123* (1), 963–970. https://doi.org/10.1021/acs.jpcc.8b11674.

(32) Ellis, C. L. C.; Javaid, H.; Smith, E. C.; Venkataraman, D. Hybrid Perovskites with Larger Organic Cations Reveal Autocatalytic Degradation Kinetics and Increased Stability under Light. *Inorg. Chem.* **2020**, *59* (17), 12176–12186. https://doi.org/10.1021/acs.inorgchem.0c01133.
(33) Charles, B.; Dillon, J.; Weber, O. J.; Islam, M. S.; Weller, M. T. Understanding the Stability of Mixed A-Cation Lead Iodide Perovskites. *J. Mater. Chem. A* **2017**, *5* (43), 22495–22499. https://doi.org/10.1039/C7TA08617B.
(34) Pool, V. L.; Dou, B.; Van Campen, D. G.; Klein-Stockert, T. R.; Barnes, F. S.; Shaheen, S. E.; Ahmad, M. I.; van Hest, M. F. A. M.; Toney, M. F. Thermal Engineering of FAPbI3 Perovskite Material via Radiative Thermal Annealing and in Situ XRD. *Nat. Commun.* **2017**, *8* (1), 14075. https://doi.org/10.1038/ncomms14075.
(35) Meng, K.; Wang, X.; Li, Z.; Liu, Z.; Qiao, Z.; Wang, C.; Hu, Y.; Li, S.; Cheng, L.; Zhai, Y.; Chen, G. Self-Passivation of Low-Dimensional Hybrid Halide Perovskites Guided by Structural Characteristics and Degradation Kinetics. *Energy Environ. Sci.* **2021**, 10.1039.D0EE03836A. https://doi.org/10.1039/D0EE03836A.
(36) Donakowski, A.; Miller, D. W.; Anderson, N. C.; Ruth, A.; Sanehira, E. M.; Berry, J. J.; Irwin, M. D.; Rockett, A.; Steirer, K. X. Improving Photostability of Cesium-Doped Formamidinium Lead Triiodide Perovskite. *ACS Energy Lett.* **2021**, *6* (2), 574–580. https://doi.org/10.1021/acsenergylett.0c02339.
(37) Ho, K.; Wei, M.; Sargent, E. H.; Walker, G. C. Grain Transformation and Degradation Mechanism of Formamidinium and Cesium Lead Iodide Perovskite under Humidity and Light. *ACS Energy Lett.* **2021**, *6* (3), 934–940. https://doi.org/10.1021/acsenergylett.0c02247.
(38) Lin; Guo; Dai; Lin; Hsu. PbI2 Single Crystal Growth and Its Optical Property Study. *Crystals* **2019**, *9* (11), 589. https://doi.org/10.3390/cryst9110589.
(39) Koutselas, I. B.; Ducasse, L.; Papavassiliou, G. C. Electronic Properties of Three- and Low-Dimensional Semiconducting Materials with Pb Halide and Sn Halide Units. 12.
(40) Ouyang, Y.; Li, Y.; Zhu, P.; Li, Q.; Gao, Y.; Tong, J.; Shi, L.; Zhou, Q.; Ling, C.; Chen, Q.; Deng, Z.; Tan, H.; Deng, W.; Wang, J. Photo-Oxidative Degradation of Methylammonium Lead Iodide Perovskite: Mechanism and Protection. *J. Mater. Chem. A* **2019**, *7* (5), 2275–2282. https://doi.org/10.1039/C8TA12193A.
(41) Stoddard, R. J.; Eickemeyer, F. T.; Katahara, J. K.; Hillhouse, H. W. Correlation between Photoluminescence and Carrier Transport and a Simple In Situ Passivation Method for High-Bandgap Hybrid Perovskites. *J. Phys. Chem. Lett.* **2017**, *8* (14), 3289–3298. https://doi.org/10.1021/acs.jpclett.7b01185.
(42) Kim, G. Y.; Senocrate, A.; Yang, T.-Y.; Gregori, G.; Grätzel, M.; Maier, J. Large Tunable Photoeffect on Ion Conduction in Halide Perovskites and Implications for Photodecomposition. *Nat. Mater.* **2018**, *17* (5), 445–449. https://doi.org/10.1038/s41563-018-0038-0.
(43) Conings, B.; Drijkoningen, J.; Gauquelin, N.; Babayigit, A.; D'Haen, J.; D'Olieslaeger, L.; Ethirajan, A.; Verbeeck, J.; Manca, J.; Mosconi, E.; Angelis, F. D.; Boyen, H.-G. Intrinsic Thermal Instability of Methylammonium Lead Trihalide Perovskite. *Adv. Energy Mater.* **2015**, *5* (15), 1500477. https://doi.org/10.1002/aenm.201500477.
(44) Singh, A. N.; Kajal, S.; Kim, J.; Jana, A.; Kim, J. Y.; Kim, K. S. Interface Engineering Driven Stabilization of Halide Perovskites against Moisture, Heat, and Light for Optoelectronic Applications. *Adv. Energy Mater.* **2020**, *10* (30), 2000768. https://doi.org/10.1002/aenm.202000768.
(45) Ouyang, Y.; Shi, L.; Li, Q.; Wang, J. Role of Water and Defects in Photo-Oxidative Degradation of Methylammonium Lead Iodide Perovskite. *Small Methods* **2019**, *3* (7), 1900154. https://doi.org/10.1002/smtd.201900154.

(46) Kim, M.; Ahn, N.; Lim, E.; Jin, Y. U.; Pikhitsa, P. V.; Heo, J.; Kim, S. K.; Jung, H. S.; Choi, M. Degradation of $CH_3NH_3PbI_3$ Perovskite Materials by Localized Charges and Its Polarity Dependency. *J. Mater. Chem. A* **2019**, *7* (19), 12075–12085. https://doi.org/10.1039/C9TA03180D.
(47) Levine, I.; Gupta, S.; Brenner, T. M.; Azulay, D.; Millo, O.; Hodes, G.; Cahen, D.; Balberg, I. Mobility–Lifetime Products in $MAPbI_3$ Films. *J. Phys. Chem. Lett.* **2016**, *7* (24), 5219–5226. https://doi.org/10.1021/acs.jpclett.6b02287.
(48) Boudart, M.; Tamaru, K. The Step That Determines the Rate of a Single Catalytic Cycle. *Catal. Lett.* **1992**, *9*, 15–22. https://doi.org/10.1007/BF00769076.
(49) Kozuch, S.; Martin, J. M. L. The Rate-Determining Step Is Dead. Long Live the Rate-Determining State! *ChemPhysChem* **2011**, *12* (8), 1413–1418. https://doi.org/10.1002/cphc.201100137.
(50) Folger, H. S. *Essentials of Chemical Reaction Engineering*; Pearson College Division, 2010.
(51) Steinfeld, J. I.; Francisco, J. S.; Hase, W. L. *Chemical Kinetics and Dynamics*, Second.; Pretence Hall: Upper Saddle River, NJ, USA, 1998.
(52) Godding, J. S. W.; Ramadan, A. J.; Lin, Y.-H.; Schutt, K.; Snaith, H. J.; Wenger, B. Oxidative Passivation of Metal Halide Perovskites. *Joule* **2019**, *3* (11), 2716–2731. https://doi.org/10.1016/j.joule.2019.08.006.
(53) Chin, D. H.; Chiericato, G.; Nanni, E. J.; Sawyer, D. T. Proton-Induced Disproportionation of Superoxide Ion in Aprotic Media. *J. Am. Chem. Soc.* **1982**, *104* (5), 1296–1299. https://doi.org/10.1021/ja00369a025.
(54) Cotton, F. A.; Wilkinson, G. *Basic Inorganic Chemistry*, 1st ed.; John Wiley & Sons, Inc: United States, 1976.
(55) Li, Q.; Chen, Z.; Tranca, I.; Gaastra-Nedea, S.; Smeulders, D.; Tao, S. Compositional Effect on Water Adsorption on Metal Halide Perovskites. *Appl. Surf. Sci.* **2021**, *538*, 148058. https://doi.org/10.1016/j.apsusc.2020.148058.
(56) Ma, C.; Park, N.-G. Paradoxical Approach with a Hydrophilic Passivation Layer for Moisture-Stable, 23% Efficient Perovskite Solar Cells. *ACS Energy Lett.* **2020**, *5* (10), 3268–3275. https://doi.org/10.1021/acsenergylett.0c01848.